

**Mechanism of recrystallization process in epitaxial GaN under dynamic stress field :  
Atomistic origin of planar defect formation**

C. R. Das,<sup>1</sup> S. Dhara,<sup>1,2,a)</sup> H. C. Hsu,<sup>3</sup> L. C. Chen,<sup>3</sup> Y. R. Jeng,<sup>4</sup> A. K. Bhaduri,<sup>1</sup> Baldev Raj,<sup>1</sup> K. H. Chen,<sup>3,5</sup> S. K. Albert,<sup>1</sup>

<sup>1</sup>Metallurgy and Materials Group, Indira Gandhi Center for Atomic Research, Kalpakkam-603102, India

<sup>2</sup>Department of Electrical Engineering, Institute for Innovations and Advanced Studies, National Chen Kung University, Tainan-701, Taiwan.

<sup>3</sup>Center for Condensed Matter Sciences, National Taiwan University, Taipei-106, Taiwan

<sup>4</sup> Department of Mechanical Engineering, National Chung Cheng University, Chia-Yi 621, Taiwan

<sup>5</sup>Institute of Atomic and Molecular Sciences, Academia Sinica, Taipei-106, Taiwan

Mechanism of recrystallization in epitaxial (0001) GaN film, introduced by indentation technique, is probed by lattice dynamic studies. A planar defect migration mechanism is evolved. ‘Pop-in’ bursts in the loading line indicate nucleation of dislocations and climb of dislocations set in plastic motion of lattice atoms under stress field at the center of indentation for the initiation of recrystallization process. Activation volume is found to be very close to the vacancy volume, supporting vacancy migration as the rate limiting factor in the process of recrystallization.

---

<sup>a)</sup> Author to whom correspondence should be addressed; electronic mail: dhara@igcar.gov.in

Presently on leave from Materials Science Division, Indira Gandhi Center for Atomic Research, Kalpakkam-603102, India

GaN is one of the most important optoelectronic semiconductors for its applications as white light source, blue diode leading to UV lithography. High dislocation density in GaN is one of the major hindrances for its application as blue laser. By adopting lateral epitaxial overgrowth (LEO) technique, a remarkably low threading dislocation (TD) density  $\sim 10^4 \text{ cm}^{-2}$  for selected region is reported in epi-GaN film [1]. Thus, reduction in residual stress by reduction in dislocation densities is one of the prime objectives for opto-electronic device applications in GaN. Recently, we have reported recrystallization of GaN under indentation [2]. Manifestation of stress for GaN in the indentation process is also reported by others [3,4].

Looking into the importance of the issue, much attention has been paid to study the defect formation mechanism in GaN [5-8]. A layer-by-layer defect formation in GaN is unanimously accepted after the detailed study by ion implantation technique [5]. In these reports, structural and optical studies reveal the defect formation process without any detailed atomistic model for its origin and dynamics. We report here the mechanism of recrystallization in wurtzite (WZ) epi-GaN film under indentation. Lattice dynamic studies by probing phonon modes reveal the possible defect migration mechanism, which influences the crystallization process. Defect nucleation and dynamics are also studied for an atomistic view of the process.

Undoped epi-layer of 6  $\mu\text{m}$  thickness (0001) GaN/ $\text{Al}_2\text{O}_3$  grown by MOCVD with TD  $< 5 \times 10^8 \text{ cm}^{-2}$  (TDI, USA) along with intrinsic carrier concentration of  $\sim 3 \times 10^{17} \text{ cm}^{-3}$  is used for the present study. The sample is indented using the micro-indenter with a Berkovich diamond tip. The data presented in this report exploits indentation conditions of load 100-400 mN; same loading-unloading rate of  $1\text{-}50 \text{ mN.s}^{-1}$  and holding time 5 s. Loads are chosen such that

penetration depth is  $\leq 20\%$  of the sample thickness, so as to avoid substrate contribution. The indentation fingerprint represents a triangle with a side length of about  $10\text{ }\mu\text{m}$ .

The structural transformation is studied close to the indented region using micro-Raman spectroscopy (Fig. 1a) using excitation wavelength of  $632.8\text{ nm}$  of He-Ne laser (probed volume  $< 1\text{ }\mu\text{m}^3$ ).  $E_2$  (high) mode at  $570\text{ cm}^{-1}$ , measured outside the indented region, resemble the reported value of epi-GaN on sapphire substrate. Inset shows the spots measured out- and insides of the indentation mark recorded in the optical microscope attached to the spectrometer. However, micro-Raman measurements inside the indented region show redshift of phonon mode gradually to  $567\text{ cm}^{-1}$  from interface region (edge of the spot) to the center of indented spot. This value is close to the calculated and measured value for  $E_2$  (high) phonon of bulk GaN and GaN nanostructure under stress free conditions [9,10]. Double peaks are observed for the interface region close to the edge of the indentation (Fig. 1a), showing contributions from both the stressed region outside and stress free region inside the indented region. Raman area mapping (outset of Fig. 1a) using spectral part of  $568\text{-}573\text{ cm}^{-1}$  shows red (bright in the grayscale) region lying outside the indented region and  $562\text{-}568\text{ cm}^{-1}$  shows Green (bright in the grayscale) region lying inside the indented region. It clearly shows that the  $567\text{ cm}^{-1}$  signal originates from the stress free region inside the indented mark and  $570\text{ cm}^{-1}$  peak originates from the stressed region of the sample. Two additional peaks at  $531\text{ cm}^{-1}$  and  $559\text{ cm}^{-1}$  (Fig. 1a) corresponding to  $A_1(\text{TO})$  and  $E_1(\text{TO})$  modes, respectively, are also observed in the indented region. According to selection rule in WZ crystal of GaN, TO phonon modes are forbidden in the backscattering geometry for the (0001) oriented planes [10]. However, small misorientations of crystallites in the indented region allow phonon modes corresponding to other crystalline orientations, as shown in the schematics (Fig. 1b) for the WZ crystal [11,12], appear in the present scattering

configuration. It can be also mentioned that the phonons (Fig. 1b) corresponding to  $E_2(\text{high})$ , and TO modes of  $A_1$  and  $E_1$  symmetries are along  $X$  and/or  $Y$  direction (confined mostly to  $XY$  plane). So, the lattice modes in the  $XY$  plane are vibrant. We have considered both the backward and right angled scattering processes, as after indentation the surface of the epi-GaN is no longer flat and in the ‘V’ grooved geometry a right angled scattering is not obscured. From the evolution of  $E_2(\text{high})$  and TO phonon modes, collected in the backscattering geometry, it seems that stress is released in the planar direction so that Raman modes along  $X$  or  $Y$  or both gets modified. Interestingly, peak  $\sim 736 \text{ cm}^{-1}$  corresponding to  $A_1(\text{LO})$  mode in the different regions close to the indentation spot (Fig. 2a) show no shift in peak position. Raman scattering configuration for the wurtzite crystal (schematic in Fig. 2b) [11,12], for phonon corresponding to LO mode of  $A_1$  symmetry is always (leaving quasi LO modes in the right angled scattering process) along  $Z$  direction (normal to  $XY$  plane). Thus with no change in peak position of  $A_1$  (LO) mode, it is obvious that lattice modes normal to  $XY$  plane remain unaltered. This is also well known that defects in GaN propagate in the planar direction. A layer-by-layer model of defect accumulation in epi-GaN is modeled from Rutherford backscattering (RBS) based channeling experiments supported by cross-sectional transmission electron microscopic imaging [5]. Thus, overall evolution of phonon modes may be due to nucleation of dislocation as reported in our earlier study [2] and release of its stress field under indentation stress to set in planar motion at the centre of indentation region by dislocation climb. Dislocation climb in the material are reported under very high hydrostatic stress due to indentation, even though test temperature is a relatively small fraction of the melting temperature of material [13]. A small peak  $\sim 707 \text{ cm}^{-1}$  peeps in the spectra collected from the regions inside the indentation. This peak can be

calculated as surface optic mode of nanocrystalline GaN [14], originating from the fresh surface inside the spot created by the indenter.

Further, we explore the role of nucleation as well as the motion of dislocation and rate limiting factors in the recrystallization process. A typical loading-unloading plot is shown (Fig. 3a) with penetration depth ~20% of the film thickness used. ‘Pop-in’ burst in the loading line (encircled in the Fig. 3) is noticed, where the indenter suddenly penetrates deeper into the material without any additional force being applied. Recent findings suggest that the origin of an initial pop-in in crystals could be explained in terms of homogeneous [15-17], or heterogeneous [18] dislocation nucleation under the penetrating tip. In general, in wurtzite epi-GaN grown in the (0001) direction, TD are of three types, with Burgers vectors ( $b$ ):  $1/3 \langle 11\bar{2}0 \rangle$  ( $a$  edge),  $\langle 0001 \rangle$  ( $c$  screw) and  $1/3 \langle 11\bar{2}3 \rangle$  [ $(a+c)$  mixed] [19]. The majority of these dislocations are  $a$  edge, whereas the  $c$  screw usually constitutes the smallest fraction [20]. The density of the  $(a+c)$ -mixed dislocations varies between that of the  $a$  edge [21] and of the  $c$  screw [20] dislocations depending on the growth conditions. However, in the nanoindentation test, with increasing load there is initially an elastic deflection in the upper surface of epi-GaN film, and then plastic deformation is typically found to associate with a discrete burst of displacement, as the indenter tip ‘pops’ into the specimen. Such suddenly indentation-induced ‘pop-in’ may cause crystallographic tilts and lattice mismatches in the epi-GaN film. These mismatches result in a high interfacial stress and the intrinsic stress in the epi-GaN film, generating TDs traverse the film to relieving structural changes.

High value of hydrostatic and shear stress are present within this plastic volume beneath the indentation and the later is responsible for the plasticity. After the indenter pressed into the material, the instant plasticity (‘pop-in’) occurs as soon as shear stress crossed the theoretical

stress. The mechanism responsible for the ‘pop-in’s appear to be associated with the nucleation and movement of dislocation sources [18,22]. The maximum shear stress ( $\tau_{max}$ ) occurring in the film at critical load,  $P_{criti}$  can be estimated [23] by

$$\tau_{max} = 0.12 \left( \frac{P_{criti} E_s^2}{R^2} \right)^{1/3} \text{-----} (1)$$

Where,  $R$  is the tip radius of curvature of the indenter,  $\tau_{max}$  is the shear stress,  $P_{criti}$  is the initial bursting load,  $E_s$  is the modulus of the material can be estimated from

$$\frac{1}{E_R} = \left( \frac{(1-\nu_{in}^2)}{E_{in}} + \frac{(1-\nu_s^2)}{E_s} \right) \text{-----} (2)$$

where  $E_R$  is reduced modulus,  $E_{in}$  (1141GPa) is indenter modulus and  $\nu_{in}$  (0.07) is indenter Poisson ratio,  $\nu_s$  is material poison ratio is 0.352. The observed value for  $P_{criti} = 10.69$  mN (Fig. 3b) for one of the studies with very low load showing distinct threshold ‘pop-in’. With  $E_s$  value of 198 GPa, as calculated from Eqn. 2 and  $R = \sim 600$  nm (measured from the SEM image),  $\tau_{max}$  can be calculated to be  $\sim 12.42$  GPa. This value is higher than the calculated theoretical shear strength  $\tau_{th} [= \mu_s/2\pi]$ , where  $\mu_s = E_s/2(1+\nu_s) = 73$  GPa], value  $\approx 11.66$  GPa to initiate ‘pop-in’.

A hardness value of  $\sim 10$  GPa is achieved in our indentation study [2] and the value is comparable to bulk value of GaN [24]. It is also observed that hardness of GaN film is also sensitive to loading rate (strain rate) as shown in Fig 4(a). At lower strain rate, hardness is found to be  $\sim 10$  GPa and increases with strain rate. Increasing hardness with strain rate can be explained with increase in dislocation density due to its multiplication [25] by shear stress component following strain gradient plasticity model [26]. Stress relaxation at the tip of the indentation can be understood from the strain rate exponent ( $m$ ) and activation volume ( $V_A$ ) analysis. These two parameters are used to determine possible deformation mechanism for a

given material. It also provides quantitative measures of the sensitivity of hardness,  $H$  to the strain rate,  $\dot{\varepsilon}$  and also provide insights to the deformation mechanisms. The engineering strain rate sensitivity can be expressed as [27]

$$m = \left( \frac{\partial \ln H}{\partial \ln \dot{\varepsilon}} \right) \text{-----} (3)$$

Where  $k_B$  is the Boltzmann constant,  $T$  is the absolute temperature.  $V_A$  can be measured by [18,27]

$$V_A = 3\sqrt{3kT} \left( \frac{\partial \ln \dot{\varepsilon}}{\partial H} \right) \text{-----} (4)$$

$m$  and  $V_A$  are calculated to be around 0.26 and  $0.3b^3$  from the linear plots of  $\ln H$  vs.  $\ln \dot{\varepsilon}$  (Fig. 4b) and  $\ln \dot{\varepsilon}$  vs.  $H$  (Fig. 4c), respectively at the peak load of 100mN. The value of  $V_A$  is comparable to the average vacancy volume ( $\sim 0.7b^3$ ) in GaN considering both Ga and N vacancy present [28]. It can be mentioned that with increase in peak load of 200 mN, the value of  $m$  decreases to 0.06 and  $V$  is found to increase to  $1.6b^3$  (Supplementary Fig. S1). It is generally accepted that high  $m$  is indicative of smaller  $V_A$  [29]. Thus, the magnitude of  $V_A$  extracted from our experiment are reflective of atomic-scale event, so one can think of point defect (vacancies) related process is the rate limiter for the plastic deformation process. Atomistic simulation studies on perfect single crystals have shown that dislocation nucleate either homogeneously [15-17], or heterogeneously [18] beneath the indenter in the material. In single crystal Pt, this value reported for homogeneous dislocation nucleation is  $\sim 0.5b^3$  [30]. Though self-diffusion is slow at ambient temperature, authors argue that raise in temperature in the material [31] beneath the indenter due to adiabatic process and high pressure gradient can cause the high diffusivity of

vacancy to the high pressure region to release the compressive stress from the material as proposed by Schuh *et al.* [18]. The vacancy concentration (considering intrinsic carrier primarily contributed from vacancy like defects) can be estimated  $\sim 10^{17} \text{ cm}^{-3}$ . Lower activation volume and high vacancy concentration suggests heterogeneous dislocation nucleation is the most probable, from the pre-existing defects such as vacancies. Homogenous dislocation loop may not be possible due to large activation [18,30] required for the process. The motion of few atoms may initiate the dislocation looping resulting multiple burst in the loading line [32]. Stress-induced crystallization has been also reported in Ge at temperature as low as 400 K [33]. Observation of in-plane phonon dynamics and low activation volume for vacancy migration suggests that climb of dislocation by vacancy is the rate limiting factor for the recrystallization process.

Thus, we address an important issue of recrystallization process in GaN under indentation stress. Heterogeneous nucleation of dislocation is evidenced in the indentation process. Heterogeneous nucleation of dislocation is originated by shear stress within the plastic zone and release of stress takes place by climb of dislocation due to high hydrostatic stress present in the plastic volume. Vacancy migration is the limiting process to initiate the recrystallization process. The mechanism of the crystallization process is clearly evaluated with lattice dynamics studies. Present study implies important clues for reducing residual stress in an epi-film, and the findings will have broad technological repercussion.

One of the author (CD) would like to thank C. Phaniraj of IGCAR, India for his valuable discussion.



## References

1. Y. Chen, *et al.*, Appl. Phys. Lett. **75**, 2062 (1999).
2. S. Dhara, *et al.*, Appl. Phys. Lett. **92**, 143114 (2008).
3. M. Giehler, *et al.*, J. Appl. Phys. **89**, 3634 (2001)
4. P. Puech, *et al.*, J. Appl. Phys. **96**, 2853 (2004).
5. S. O. Kucheyev, J. S. Williams, S. J. Pearton, Mater. Sci. and Engg. R-Reports **33**, 51 (2001).
6. J. Elsner, *et al.*, Phys. Rev. Lett. **79**, 3772 (1997); Z. Liliental-Weber, *et al.*, Phys. Rev. Lett. **83**, 2370 (1999).
7. K. H. Chow, *et al.*, Phys. Rev. Lett. **85**, 2761 (2000); K. Saarinen, *et al.*, Phys. Rev. Lett. **79**, 3030 (1997).
8. S. J. Pearton, *et al.*, J. Appl. Phys. **86**, 1 (1999).
9. V. Y. Davydov, *et al.*, Phys. Rev. B **58**, 12899 (1998).
10. T. Azuhata, *et al.*, J. Phys.: Condens. Matter. **7**, L129 (1995).
11. C. A. Arguello, D. L. Rousseau, and S. P. S. Porto, Phys. Rev. **181**, 1351 (1969).
12. H. Harima, J. Phys.: Condens. Matter **14**, R967 (2002).
13. O. Sahin, *et al.*, Physica B **399**, 87 (2007).
14. R. Rupp, and R. Englman, Rep. Prog. Phys. **33**, 149 (1970); Surface optic mode corresponding to  $E_1$  character of GaN can be calculated for spherical nanoclusters with reported static and high frequency dielectric constants of 10.4 and 5.8 and air as matrix.
15. J. Li *et al.*, Nature (London) **418**, 307 (2002).
16. I. Szlufarska, A. Nakano, and P. Vashista, Science **309**, 911 (2005).
17. A. Guldstone, K. J. Van Vliet, and S. Suresh, Nature (London) **411**, 656 (2001).
18. C. A. Schuh, J. K. Mason, and A. C. Lund, Nat. Mater. **4**, 617 (2005); J. K. Mason, A. C.

- Lund, and C. A. Schuh, Phys. Rev. B **73**, 054102 (2006).
19. F. A. Ponce, *et al.*, Appl. Phys. Lett. **69**, 770 (1996).
  20. W. Qian, *et al.*, Appl. Phys. Lett. **67**, 2284 (1995).
  21. D. Wang, M. Ichikawa, and S. Yoshida, Philos. Mag. Lett. **82**, 119 (2002).
  22. C. L. Kelchner, S. J. Plimpton, and J. C. Hamilton, Phys Rev B **58**, 11085 (1999).
  23. R. Thokala, J. Chaudhuri, Thin Solid Films **266**, 189 (1995).
  24. M. D. Drory, *et al.*, Appl. Phys. Lett. **69**, 4044 (1996).
  25. H. Siethoff, Mater Sci Engg. A **386**, 68 (2004).
  26. W. D. Nix, and H. Gao, J. Mech Phys. Solid, **46**, 411 (1998).
  27. A. A. Elmustafa, and D. S. Stone, J. Mech. Phys. Solid **51**, 357 (2003).
  28. C. D. Gu, *et al.*, J. Phys. D: Appl. Phys. **40**, 744 (2007).
  29. J. Neugebauer and C. G. Van de Walle, Phys Rev B **50**, 8067 (1999).
  30. M. A. Tschopp, and M. D. McDowell, J. Mech. Phys. Solids. **56**, 1806 (2008).
  31. C. H. Tsai, S. R. Jian and J. Y. Juang, Appl. Surf. Sci. **254**, 1997 (2008).
  32. L. Zuo, A. H. W. Ngan, and G. P. Zheng, Phys. Rev. Lett. **94**, 095501 (2005)
  33. D. Shahrjerdi, *et al.*, Thin Solid Films **427**, 330 (2003).

## Figure captions

Fig. 1. (Color online) a) Micro-Raman spectra for epi-GaN outside and different regions inside the indentation spot. Inset shows corresponding optical image of the indentation spot. Area mappings of outside and inside of the indentation spot, using different spectral regions indicated in the picture, are shown at the outset. b) Different Raman scattering configuration for wurtzite crystal in the backward (top) and right angled (bottom) direction corresponding to  $E_2$ , and TO modes of  $E_1$  and  $A_1$  symmetries. The incident and scattered direction of exciting photon is represented by  $k_i$ , and  $k_s$ , respectively and  $q$  is the direction of phonon scattering. Small arrows and the crossed circle are the direction of polarization, with later directing perpendicular to the plane of the paper (*Drawn after Fig. 6 of Ref. [11] and applied for permission from American Physical Society*)

Fig. 2. (Color online) a) Micro-Raman spectra for epi-GaN outside and different regions inside the indentation spot. Inset shows corresponding optical image of the indentation spot. b) Raman scattering configuration for wurtzite crystal in the backward scattering direction corresponding to LO mode of  $A_1$  symmetry. The incident and scattered direction of exciting photon is represented by  $k_i$ , and  $k_s$ , respectively and  $q$  is the direction of phonon scattering. Small arrows and the crossed circle are the direction of polarization, with later directing perpendicular to the plane of the paper (*Drawn after Fig. 6 of Ref. [11] and applied for permission from American Physical Society*)

Fig. 3. Variation of load and depth of indentation at peak loads of (a) 200 mN and (b) 45 mN

Fig. 4 (a) Variation hardness with indentation strain rate. Typical (b) log-log plot of hardness vs strain rate, and (c) log (indentation strain rate) vs hardness plot for the peak load of 100mN

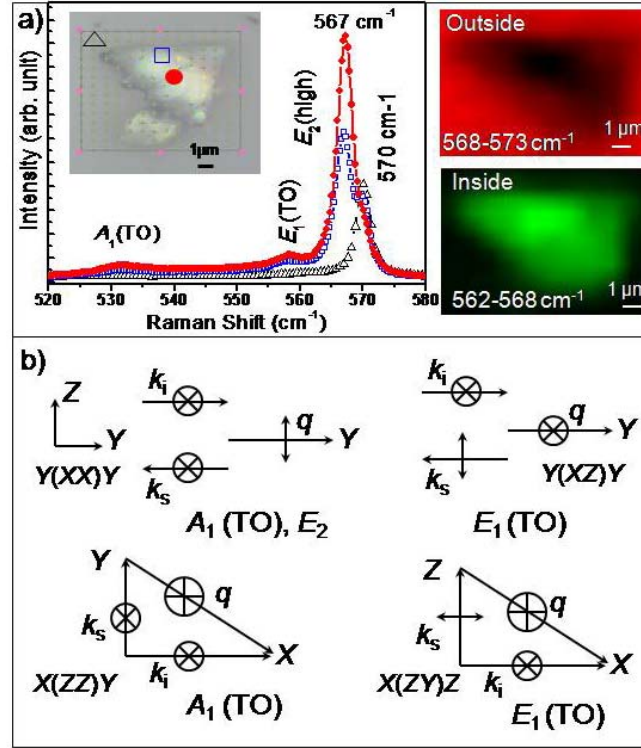


Fig. 1

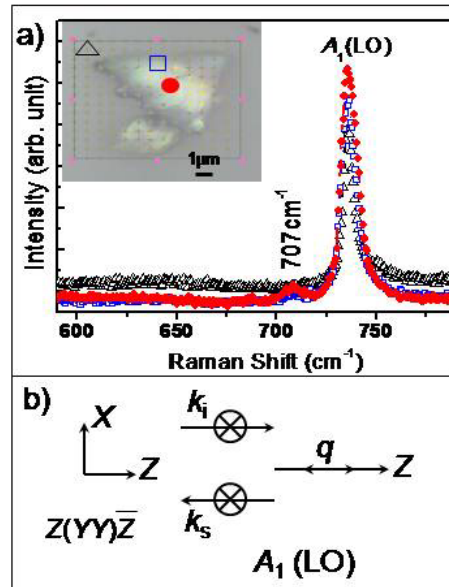


Fig. 2

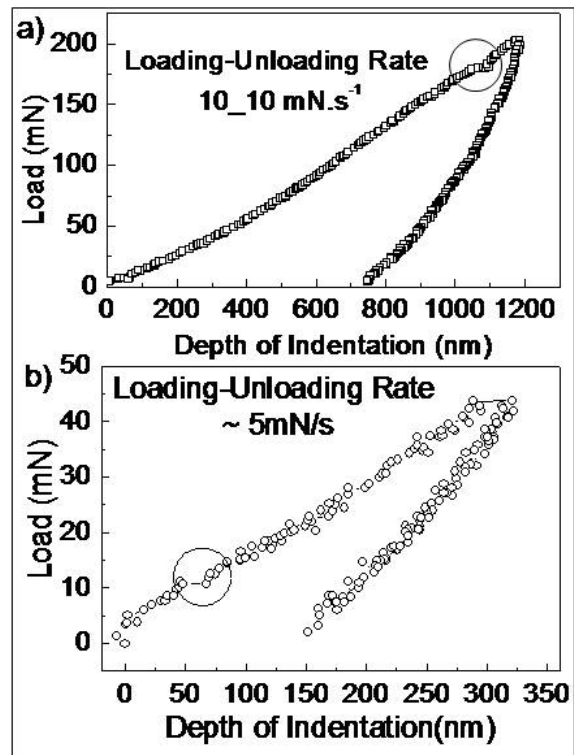


Fig. 3

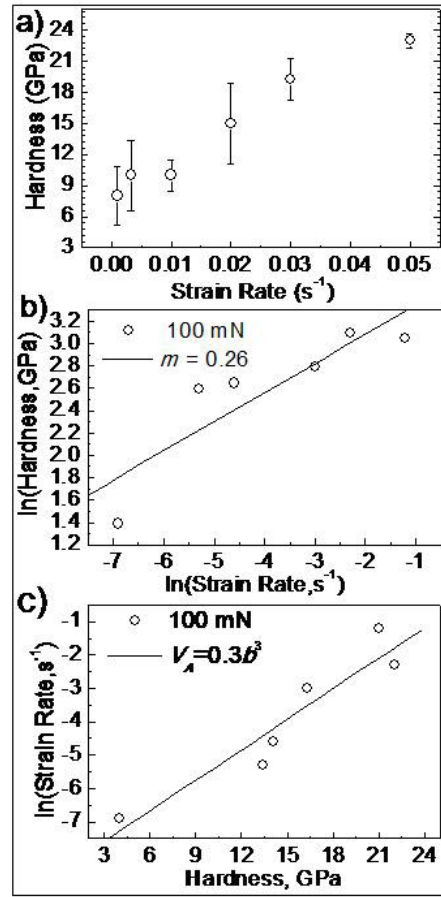


Fig. 4

## Supplementary

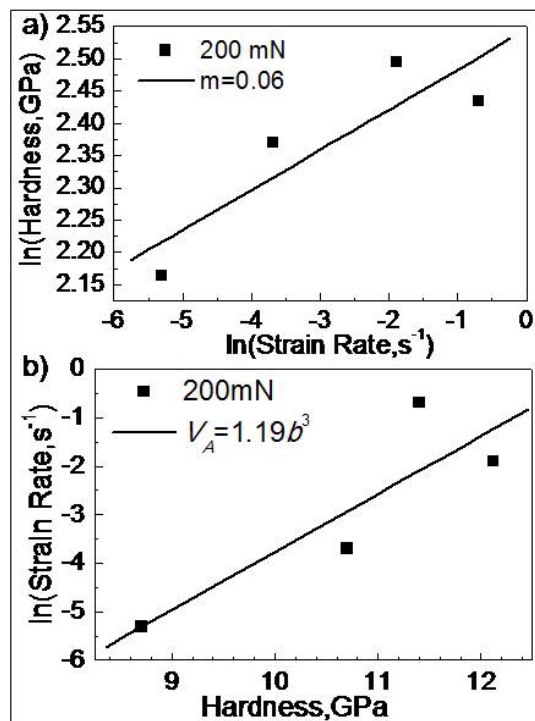


Fig. S1. Typical (a) log-log plot of hardness vs strain rate, and (b) log (indentation strain rate) vs hardness plot for the peak load of 200mN